ELSEVIER

Journal of Hydrology 231–232 (2000) 295–307

Journal of Hydrology

www.elsevier.com/locate/jhydrol

Numerical simulation of experimental gravity-driven unstable flow in water repellent sand

J.L. Nieber[a], T.W.J. Bauters[b], T.S. Steenhuis[b], J.-Y. Parlange[b]

[a]*Department of Biosystems and Agricultural Engineering, University of Minnesota, 1390 Eckles Ave., St.Paul, MN 55108, USA*
[b]*Department of Agricultural and Biological Engineering, Cornell University, Riley-Robb Hall, Ithaca, NY 14853, USA*

Received 12 December 1998; accepted 13 August 1999

Abstract

Laboratory experiments related to gravity-driven unstable flows in water repellent porous media contained in two-dimensional chambers have been reported [Bauters, T.W.J., DiCarlo, D.A., Steenhuis, T.S., Parlange, J.-Y., 1998. Preferential flow in water-repellent sands. Soil Sci. Soc. Am. J. 62, 1185–1190]. These experiments demonstrate that water repellency has a significant impact on the stability of flow. As a follow up to these experiments, numerical solutions of the Richards equation for a two-dimensional domain are derived to examine the effect of water repellency on flow characteristics. Of particular interest is the development of gravity-driven unstable flow conditions caused by water repellency. The degree of water repellency of the porous medium is manifested in the water saturation—capillary pressure and water saturation—hydraulic conductivity relationships for the porous medium. To derive the numerical solutions, parameters closely representing the flow domain boundary conditions and the porous medium properties in the experiments of Bauters et al., were employed. In this paper we present the results of simulations for two cases: a water wettable sand and an extremely water repellent sand. The numerical solution for the water wettable sand led to a stable flow condition, while for the water-repellent sand the flow was unstable as manifested by the development of a single finger of flow. A new feature of these modeling results, in comparison to previous modeling results for gravity-driven unstable flow, is that the water pressure inside the finger core is positive. In testing the numerical solutions we compared the solution results to the laboratory results in terms of flow patterns, water pressure at a single reference point, and wetting front velocity. The degree of agreement between the laboratory results and the numerical solutions in terms of these measures is quite good.

Keywords: Water repellent soils; Unstable flow; Finger flow; Numerical modeling; Soil water hysteresis

1. Introduction

Preferential flow of water is known to occur in soils and can lead to fast transport of harmful chemicals to underlying ground water resources. Also, the resulting lack of interchange between the composite soil and the preferential flow pathways can result in a reduced amount of plant available nutrients and water in the root zone.

The four recognized forms of preferential flow are the processes of macropore flow, gravity-driven unstable flow, funnel flow, and heterogeneity-driven flow. Macropore flow processes generally occur in soils of silt or clay texture and relate to flows in non-capillary pores (Beven and Germann, 1982). Gravity-driven unstable flow processes, or fingered flow processes, generally occur in soils of sandy texture, but also have been observed to occur in water repellent fine textured soils (Dekker and Ritsema, 1996). Funnel flow occurs in sandy soils where inclining layers behaving as capillary barriers direct water into concentrated channels of flow (Kung, 1990).

0022-1694/00/$ - see front matter
PII: S0022-1694(00)00202-X

Heterogeneous flow occurs in soils where the heterogeneity has a strong spatial correlation (Roth, 1995; Birkholzer and Tsang, 1997). This paper deals with the preferential flow processes related to gravity-driven unstable flow.

Gravity-driven unstable flows in water repellent field soils have been observed to occur by numerous researchers. A few of the reports in which observations are presented include those by Jamison (1945), Hendrickx et al. (1993), Ritsema et al. (1993), Ritsema and Dekker (1994), and Dekker and Ritsema (1996). Modeling of unstable flow in water repellent soils has been reported by Van Dam et al. (1990), De Rooij (1995), De Rooij and De Vries (1996), Ritsema et al. (1998) and Nguyen et al. (1999).

As outlined by Raats (1973), the process of gravity-driven unstable flow can occur in soils when the following conditions are met: (1) the saturated hydraulic conductivity increases with depth; (2) the soil is water repellent; and (3) air pressure builds up at the wetting front of infiltrating water. For all of these conditions, the wetting front slows and the front becomes unstable, manifested by the breaking of the front into discrete fingers. Associated with the slowing of the wetting front is the reversal of the pressure gradient. For stable conditions the pressure gradient is downward, while at incipient instability of the front the pressure gradient turns upward and this persists within the fingers.

In this paper we will present a modeling analysis of gravity-driven unstable flow for the condition of water repellent sand. Laboratory experiments performed by Bauters et al. (1998) on sands at two levels of water repellency are analyzed with the numerical solution method presented by Nieber (1996). One level of repellency is that of perfectly water wettable sand, that is, the repellency is absent from the sand material. For the other level the repellency is classified as extreme. In this analysis we show the effect of the presence of water repellency on the characteristics of finger formation and propagation.

The only study related to modeling unstable flow in water repellent soils, comparable to the present one, is that presented by Nguyen et al. (1999). In that study Nguyen et al. showed the simulation of unstable flows in a slightly water repellent field soil, and compared the simulated results with field observed fingered flow. The present study differs from this earlier study in that the results of a laboratory experiment, in which much more detailed measurements are available are used to test the flow simulation model, instead of using field data. In addition, the present study examines a case of a porous medium with extreme water repellency in contrast to the slight water repellency examined by Nguyen et al.

2. Laboratory experiments

Experiments with water wettable and water-repellent sands were reported by Bauters et al. (1998). In these experiments a two-dimensional slab model (0.45 m wide by 0.575 m high) was used to study the characteristics of flow instability by measuring water saturation distributions over the entire chamber, and water pressures at specific points within the domain. The water saturation distributions were measured using the light transmission methods described by Glass et al. (1989b). This method yields high-resolution data on water saturation and facilitates the study of flow fingering in detail. The water pressures were measured with rapid response tensiometers placed in a horizontal linear array at a height in the chamber of 0.32 m.

Silica sand was used in the experiments. The particle size distribution for this silica sand is presented in Table 1. In previous experiments on unstable flow (Glass et al. 1989a,b; Selker et al., 1992; Liu et al. 1994) the sands used had quite narrow particle size distributions. For instance, sand with particle size from the classes of 20–40 sieve sizes might be used. These previous experiments demonstrated that sands with narrow particle size distributions tend to promote unstable flow conditions, even when the individual sand grains are water wettable. In these earlier

Table 1
Particle size distribution for blasting silica sand

Mesh size	Screen opening (mm)	% Retained	% Cumulated
20	0.840	Trace	Trace
30	0.590	0.8	0.8
40	0.425	14.1	14.9
50	0.297	38.6	53.5
70	0.212	28.4	81.9
100	0.149	11.0	92.9
Through	<0.149	7.1	100.0

experiments it was found that for application rates less than the saturated hydraulic conductivity and initially air-dry condition, the flow would be unstable. The water application rate and the initial moisture content of the sand were both found to be important factors controlling the stability of the flow.

In contrast to those sands with uniform particle size distributions, the sand displayed in Table 1 has a fairly wide particle size distribution. When the grains of this sand composite are water wettable, it is expected that the flow will be stable, at any water application rate and initial water content. The purpose of the experiments reported by Bauters et al. (1998) was to determine whether water repellency of the sand grains would lead to unstable flow conditions as hypothesized by Raats (1973).

The silica sand was first made completely water wettable by repeated washing with acetic acid and distilled water. To create water-repellent sand a mass of the water wettable sand was treated with octadelcyltrichlorasilane dissolved in an ethanol solution. After drying, the sand grains treated with this solution had a water-repellent surface. Different amounts of water wettable sand were then mixed with the water-repellent sand to produce different degrees of water repellency as quantified by the water drop penetration time (WDPT) test. The percentages (by weight) of water repellent sand mixed with the water wettable sand were 0, 3.1, 5.0, 5.7 and 9.0%. For these, the degrees of water repellency as measured by the WDPT test were wettable ($<$5 s) for 0%, slightly water repellent (5–60 s) for 3.1%, severely water repellent (600–3600 s) for 5.0%, and extremely water repellent ($>$3600 s) for both 5.7 and 9.0%.

3. Water retention properties of experimental sand

The hysteretic water retention properties of the experimental sand were determined directly by gravimetric sampling within the experimental chamber (Bauters et al., 1998). The main wetting relation between water saturation and capillary pressure was determined by a capillary rise experiment. The capillary rise experiment was performed by setting a fixed head of water near the bottom of the chamber and allowing the water to infiltrate upwards into the chamber. After 24 h the chamber was taken apart and the sand was sampled at various heights, and the water content determined gravimetrically. The height of the sample above the fixed head elevation was used to quantify the capillary pressure. For samples taken above the fixed head level the capillary pressure is positive, while it is negative for samples taken below this elevation. Two columns of samples were taken for each level of water repellency treatment.

The water saturation—capillary pressure relation for the main drainage curve was derived by saturating the chamber at a slow rate from the bottom of the chamber, and then allowing the chamber to drain freely. Again, samples were taken and water content was measured gravimetrically. The height at which a sample was taken above the bottom of the chamber was assumed to be equal to the capillary pressure. Two columns of samples were taken for the main drainage curve analysis for each level of water repellency treatment.

The water saturation—capillary pressure relations for the main drainage curve for the various levels of water repellency are illustrated in Fig. 1. Each of the curves shown is the average of the results from the two columns of samples acquired for each treatment. It is observed that the curves for the water-repellent

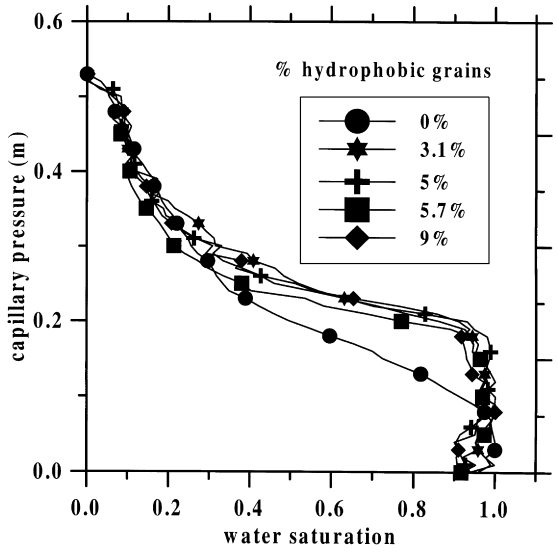

Fig. 1. Main drainage curve for the water saturation—capillary pressure relation for different levels of water repellency.

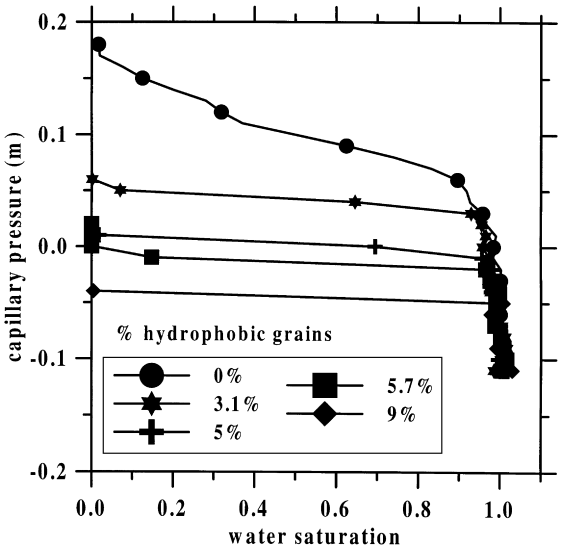

Fig. 2. Main wetting curve for the water saturation—capillary pressure relation for different levels of water repellency.

sands are very similar. Near saturation, the curves are nearly identical, while there are some differences at saturations less than about 40%. There does not seem to be any consistent trend with respect to the degree of water repellency. The shape of the water saturation—capillary pressure relations for the water-repellent sands is very similar to those expected for a coarse textured media. The shape of the curve for the water wettable sand is more representative of what one might expect for a sand with the composite texture given in Table 1. It is interesting that the water wettable sand has an air-entry value of about one-half of those for the water repellent sands. It was reported by Bauters et al. (2000) that the surface tension of the water in the water repellent sand treatments was greater than that for the water wettable sand treatment. Apparently the addition of the octadelcyltrichlorasilane to the sand increases the surface tension of water.

We should note here that some of the experimentally determined water saturations plotted in Fig. 1 for capillary pressures less than the air-entry capillary pressure are less than 100%. This is unexpected. Bauters et al. (1998) explain this as being due to the entrapment of air during the water filling processes prior to the drainage experiment. Apparently this air was not able to escape from the experimental chamber during the time frame of the water retention experiment.

The water saturation—capillary pressure relations for the main wetting curves are presented in Fig. 2. The curve for the water wettable sand has the gradual shape that is expected for a sand with the composite texture given in Table 1. The water entry capillary pressure for the water wettable sand is about 0.17 m (-0.17 m water pressure). In sharp contrast to this are the curves for the water-repellent sands. For these sands the relation is quite steep, with water entry capillary pressure decreasing significantly as the degree of water repellency increases. For the slightly water repellent sand the water entry capillary pressure is 0.055 m, while for the extremely water repellent sand the water entry capillary pressure is about -0.045 m. This water entry capillary pressure for the extremely water repellent sand means that the wetting of the sand requires a positive water pressure of at least 0.045 m.

The Van Genuchten (1980) water saturation—capillary pressure equations were fitted to the measured data using RETC (RETention Curve, Van Genuchten et al., 1991). The parameters for these equations for the water wettable sand and the extremely water repellent sand are summarized in Table 2. The α and n parameters are defined as: α_{md} and n_{md} are for the main drainage curve, α_{mw} and n_{mw} are for the main wetting curve, and α_{bws} is for the boundary wetting scanning curve. The other parameters for both sands were saturated hydraulic conductivity, $K_s = 2.82$ m/h; saturated volumetric water content, $\theta_s = 0.40\ m^3/m^3$; residual volumetric water content, $\theta_r = 0.04\ m^3/m^3$ and air-dry volumetric water

Table 2
The α and n parameters for the Van Genuchten equations for the wettable sand and the extremely water repellent sand

Case	α_{md} (m^{-1})	n_{md}	α_{mw} (m^{-1})	n_{mw}	α_{bws} (m^{-1})
Water wettable sand	5.63	3.48	10.75	4.99	11.26
Extremely water repellent sand	3.95	6.36	24.4	18.8	7.90

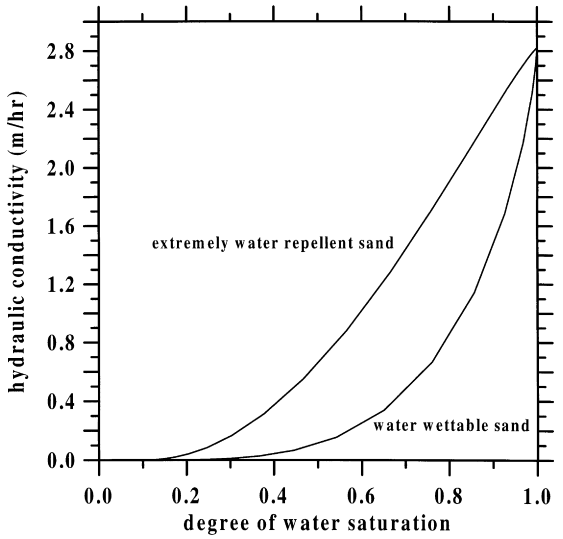

Fig. 3. Relationship between water saturation and hydraulic conductivity for the water wettable sand and the extremely water repellent sand.

content, $\theta_{\text{air-dry}} = 0.001\ \text{m}^3/\text{m}^3$. The value of n for the boundary wetting scanning curve was taken to be the same as the main drainage curve, and the value of α_{bws} was assigned a value of 2 α_{md}. Parker (1989) reported that for a good approximation of α_{bws} one can use 2 times the value of α_{md}.

The unsaturated hydraulic conductivity functions for the water wettable sand and the water-repellent sand will be different. This difference is reflected not only in the different Van Genuchten parameters, but also in the fact that the contact angle for the extremely water repellent sand is $>90°$ (Bauters et al., 2000), while the contact angle for the water wettable sand is $<90°$. As described by Bauters et al., when the contact angle is $>90°$ the pore filling sequence is reversed from that for the case where the contact angle is $<90°$.

The Van Genuchten (1980) hydraulic conductivity function for a porous medium with a contact angle $<90°$ is given by $K = K_s(S_e)^{0.5}[1 - (1 - (S_e)^{1/m})^m]^2$, where S_e is the effective saturation and $m = 1 - (1/n)$. The hydraulic conductivity function for a porous medium with a contact angle $>90°$ is the same function given by Parker (1989) for a nonaqueous fluid in a water wettable porous medium, that is, $K = K_s(S_e)^{0.5}[1 - (1 - S_e)^{1/m}]^{2m}$. Applying these two equations to the water wettable and the water repellent sand, and using $m = 1 - (1/n_{\text{md}})$, leads to the functions shown in Fig. 3. It is observed that except at the endpoints of the two functions, the water-repellent sand has a significantly higher hydraulic conductivity than the water wettable sand.

4. Flow simulation model and simulated conditions

The process examined in the laboratory experiment was one of variably saturated flow in porous media. This process can be described by the Richards equation for the flow of water in unsaturated porous media. In the present case we can assume that the air pressure in the porous media is in equilibrium with the atmosphere, and therefore it is possible to ignore the potential effects of viscous drag caused by flowing air. This allows us to treat the flow process with just the Richards equation for water, while if viscous effects of air were important, we would have to include another Richards equation to account for the air phase.

A numerical simulation model that facilitates the numerical solution of the Richards equation for unstable flow conditions has been described by Nieber (1996). The main features of this model are:

1. A globally mass conservative solution using bilinear finite elements to discretize the space domain, and implicit finite difference scheme to discretize the time domain.
2. Van Genuchten (1980) equations to describe the water saturation—capillary pressure relationship and the water saturation—hydraulic conductivity relationship.
3. A Mualem (1974) independent domain hysteresis model to describe the process of capillary hysteresis in the water saturation—capillary pressure relationship.
4. An internodal conductivity-weighting scheme to more accurately represent the hydraulic conductivity at the infiltration front. In the present study an upstream weighting factor (Nieber, 1996) of -0.95 was used for both the stable and the unstable flow simulations.This weighting factor actually yields a downstream weighting effect.

A limitation of the current model is that the

hysteresis process is applied only to the hysteresis loop that exists between the main drainage curve and the boundary wetting scanning curve. Thus, if during a wetting process along the main wetting curve the process does not reach saturation, and then begins to drain, the drainage process continues (back down) along the main wetting scanning curve. To date we have not adapted the Mualem (1974) model to produce a primary drainage scanning curve starting from the main wetting curve, except for drainage from saturation, in which case the drainage occurs along the main drainage curve. We intend to put such a drainage process into future versions of the numerical solution. As will be seen later, leaving out this primary drainage process leads to more complete drainage of the fringes of fingers and thereby lower saturation, while if the process had been included these fringes would not drain as readily.

The problem at hand involves the simulation of flow in the laboratory chamber described above and by Bauters et al. (1998). The flow domain selected for analysis has dimensions of 0.575 m height and 0.45 m width. Water is applied to the top boundary at the low rate of 0.096 m/h; this rate is equivalent to the rate (0.16 cm/min) used in one series of experiments reported by Bauters et al. The side boundaries of the domain are considered impervious and the bottom boundary is treated as a free drainage boundary. A schematic view of the flow domain, indicating the boundary conditions is presented in Fig. 4a. This flow region was subdivided into a uniform grid

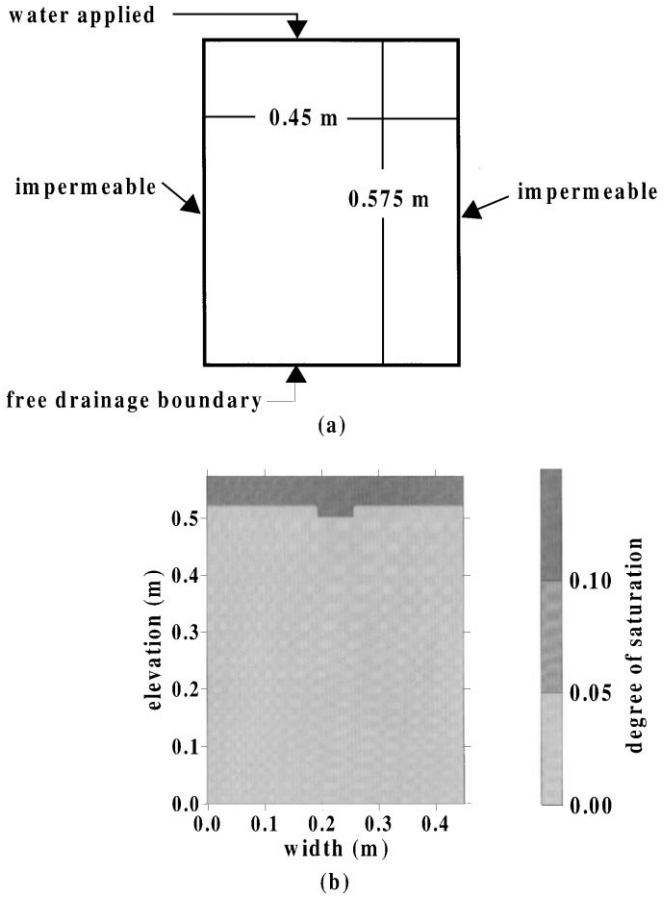

Fig. 4. Illustration of the flow region used for the numerical solutions. (a). Boundary conditions for the flow region. (b) Initial conditions for the flow region.

of 10,556 nodes. Time steps are determined automatically by the numerical simulation code and generally ranged from 3.6 to 36 s.

In the experiments of Bauters et al. (1998), precautions were taken to eliminate viscous air effects by providing sufficient escape holes for air in the sides of the chamber. This condition validated our assumption of single-phase flow.

A single reference point was located at an elevation of 0.30 m above the bottom of the chamber. This reference point was used to provide temporal pressure and saturation data at that reference location. In the laboratory experiment the pressure data were acquired at an elevation of 0.32 m. The simulated water pressure and measured water pressure at these respective locations will be used to make a quantitative comparison between the numerical and experimental results.

The initial condition for the simulations is illustrated in Fig. 4b. The region is specified to be air-dry initially, except for a 0.05 m layer at the top of the domain, with a small perturbation at the bottom-center of this layer. This top layer is assumed to have been moistened by a previous rainfall event, and subsequently dried through the top boundary by the processes of evaporation or transpiration. Thus, upon rewetting, the hysteresis pressure-saturation pathway for the sand in the layer will be a primary wetting scanning curve (Mualem, 1974). For the initially air-dry sand the hysteresis pressure-saturation pathway will be the main wetting curve.

The initial perturbation is placed onto the bottom of the layer to control the location of any fingers that might form when the conditions for unstable flow are met. If the conditions for flow instability are met, then the perturbation will grow with time and the wetting front will be considered unstable. Otherwise, the initial perturbation will dissipate and the infiltration front will move as a stable front.

5. Results and discussion

Results from the numerical simulations of flow in the two-dimensional chamber for the cases of water wettable sand and extremely water repellent sand will be presented in this section. As the simulation results are presented, reference will be made to the experimental results to indicate the degree of agreement between the numerical and simulated results.

The distribution of water saturation in the case of the water wettable sand is presented in Fig. 5. For this case, the wetting front is observed to remain stable. The initial perturbation is observed to grow wider and a bit longer as time progresses, but the growth is not a manifestation of flow instability, but instead due to diffusion of the perturbation. In a separate simulation (not shown here) for the water wettable case, where no initial perturbation was present, the wetting front was found to be completely horizontal for all time.

In the laboratory experiment, Bauters et al. (1998) reported that for the water wettable sand, the wetting front spanned the entire width of the flow chamber, indicating a stable flow condition. They reported an average front velocity of 0.6 cm/min. The simulated stable wetting front reached the bottom of the flow domain at about 3960 s. For the flow duration through the initially air-dry medium (about 3600 s) the average front velocity is found to be about 0.85 cm/min. For the simulation of the stable case without the initial perturbation (not shown here), the front velocity was also about 0.85 cm/min.

In contrast to the case of the water wettable sand, the water-repellent sand produces a distinctly unstable flow profile. The simulated results for this case are illustrated in Fig. 6. For this case the initial perturbation grows with time, and does not diffuse as it did for the water wettable case. The water saturation within the finger decreases with height above the fingertip. This distribution of water saturation is typical of those found experimentally in fingered flow (Liu et al., 1994).

The shape of the fingertip at the point where the finger joins the bottom boundary is similar to that shown by Liu et al. (1994) for the case where the finger moves from an air-dry soil into an underlying moist soil. In their experiment Liu et al. showed that when the finger touches the moist soil, the front is accelerated into the moist soil, thereby narrowing the finger width just above the interface between the dry and moist soil. In the present case there is no moist soil underlying the bottom boundary, but there is no resistance to flow either. Once the finger breaks through the bottom boundary, the flow is no longer resisted at the front and the flow velocity is accelerated locally at the tip. The finger width is therefore reduced near the bottom boundary.

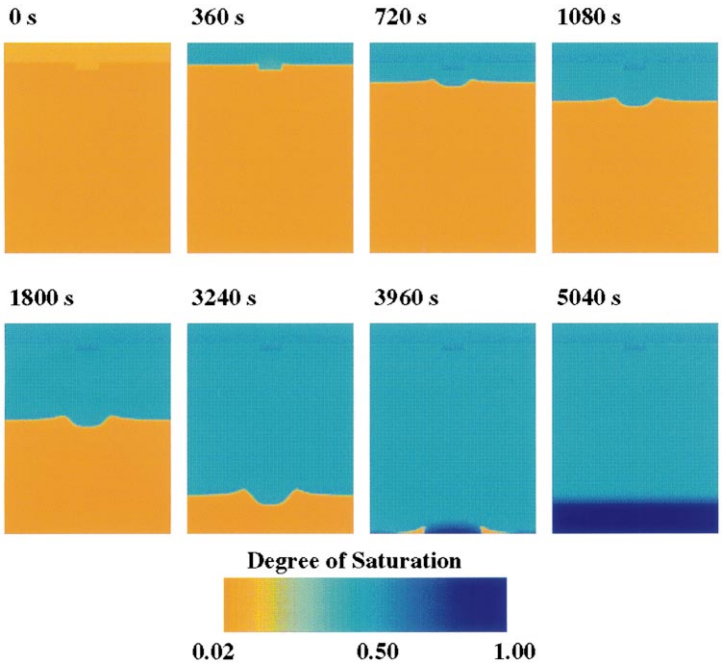

Fig. 5. Numerically simulated distributions of water saturation in the flow domain at selected times, for the case of the water wettable sand.

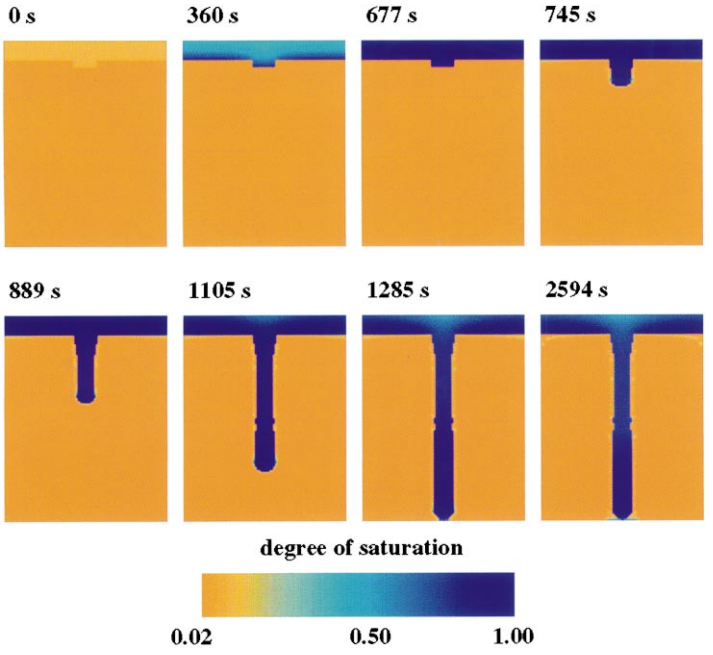

Fig. 6. Numerically simulated distributions of water saturation in the flow domain at selected times, for the case of the extremely water repellent sand.

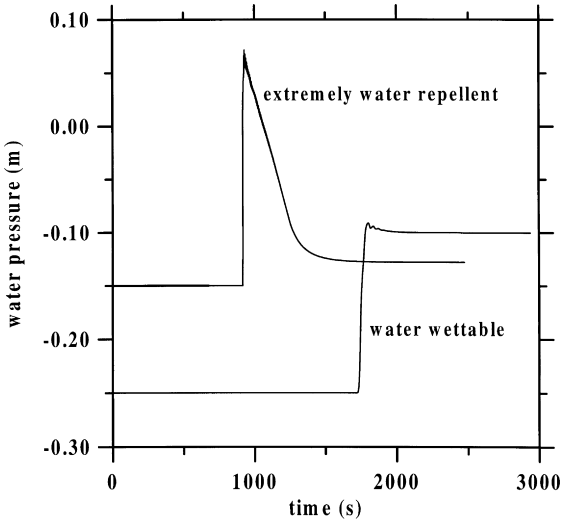

Fig. 7. Numerically simulated variation of water pressure along the midplane of the flow domain at 0.3 m elevation for the case of the water wettable sand and the extremely water repellent sand.

The finger reached the bottom boundary at 1250 s. The finger was initiated at about 673 s. Thus, the travel time for the finger is about 577 s, leading to an average front velocity of 5.3 cm/min. Bauters et al. (1998) reported an average front velocity of 5.5 cm/min. The width of the finger shown in Fig. 6 is about 0.05 m. The experimental width reported by Bauters et al. was 0.071 m.

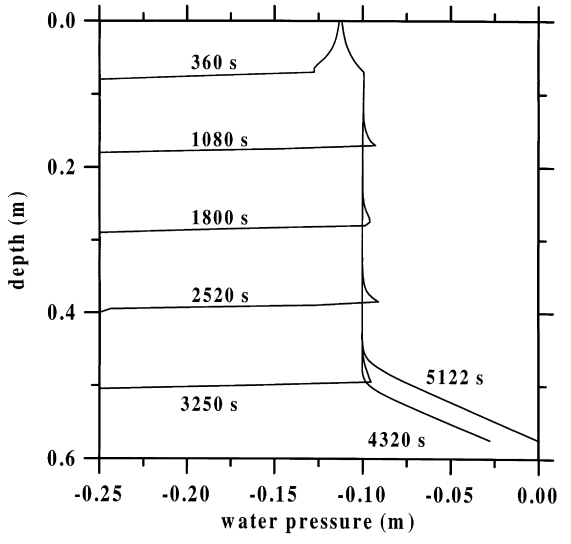

Fig. 8. Numerically simulated distributions of water pressure along the midplane of the flow domain for selected times, for the case of the water wettable sand.

While it may appear that the width of the finger is directly related to the width of the initial perturbation, this is not the case. Actually, the finger width in this case is slightly smaller than the initial perturbation, 0.05 versus 0.06 m. In many tests with the numerical model we have found that if the initial perturbation is narrower than the correct finger width the resulting finger will be wider than the initial perturbation. Likewise, if the initial perturbation is wider than the correct finger width, the resulting finger will be narrower than the initial perturbation.

Bauters et al. (1998) presented plots of water pressure measured at an elevation of 0.32 m within the laboratory chamber. The simulated water pressures at an elevation of 0.30 m, for both the water wettable case and the water repellent case are plotted in Fig. 7. The water pressure for the water wettable sand was initially at −0.25 m and the wetting front reached the reference point at 1725 s. The water pressure then increased relatively quickly and became steady at −0.10 m. This steady value is fairly close to the value of −0.12 m reported by Bauters et al. The small blip that occurred in the simulated water pressure just prior to it becoming steady is due to the downstream weighting of the hydraulic conductivity used in the numerical solution. This blip does not appear in the measurements of Bauters et al. and so can be assumed to be an artifact of the numerical simulation. The downstream weighting is a necessity for the simulation of unstable flow, and to be consistent between the simulations the downstream weighting factor was kept the same between the water wettable case and the water-repellent case.

For the water repellent case the wetting front reached the reference point at 916 s. The water pressure increased rapidly, and for this case it became positive, reaching a maximum value of 0.071 m. After peaking, the water pressure at the reference point dropped rapidly and then levelled out to a value of −0.13 m. The peak water pressure reported by Bauters et al. was 0.056 m, while the steady state water pressure was −0.12 m. The trend in water pressure shown in Fig. 7 is exactly similar to that found by Bauters et al. (1998) for the water repellent case, and by Selker et al. (1992) for a water wettable sand

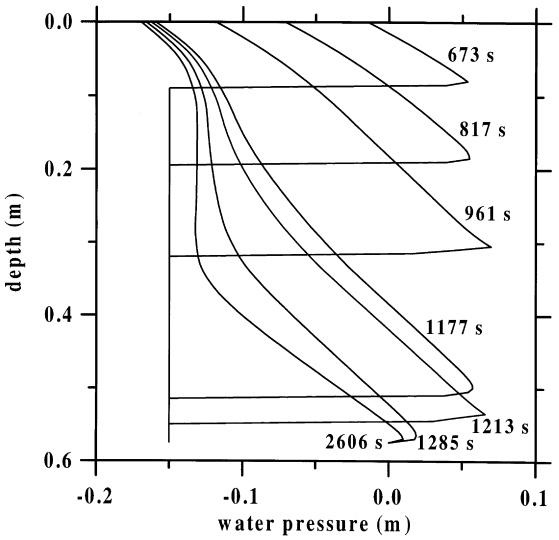

Fig. 9. Numerically simulated distributions of water pressure along the midplane of the flow domain for selected times, for the case of the extremely water repellent sand.

having a narrow particle size distribution. The difference between the Bauters et al. result and the Selker et al. result is that for the Selker et al. experiment the peak water pressure was about −0.055 m. This difference is expected since a water wettable sand will have a water entry pressure value less than zero.

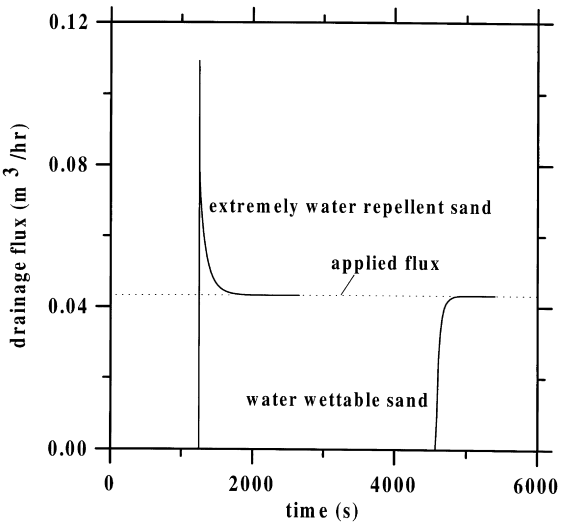

Fig. 10. Drainage flux at the bottom of the flow domain for the water wettable case and the extremely water repellent case. The flux applied at the top of the flow domain is indicated.

The distribution of pressure along the vertical midplane of the flow domain for each of the flow cases is illustrative of the different characteristics between the stable and unstable flow conditions. The pressure distribution for the water wettable case is illustrated in Fig. 8. For the part of the domain below the initially wetted layer the water pressure profile is seen to be fairly uniform down to the wetting front. The small blip in the pressure distribution at the wetting front is clearly seen here, and as described above this is caused by the practice of using downstream weighting of the nodal hydraulic conductivities.

The pressure distributions for the water-repellent case, shown in Fig. 9, indicate that conditions approach hydrostatic conditions within the finger domain during the initial phases of finger formation. The low hydraulic gradient, 0.33, afforded by this pressure profile is part of the cause for the high water saturation in the finger, in comparison to the flow for the stable case where the hydraulic gradient is close to 1. Of course, the fact that all of the applied water has to flow through the finger, rather than being spread throughout the domain is the other cause for the higher saturation. Once the finger reaches the bottom boundary and water begins to drain from the finger, the pressure profile approaches a uniform pressure condition in the upper part of the flow domain.

For the water wettable case the sand is unsaturated behind the front, while for the water-repellent sand, as for any unstable flow situation, the water saturation is 100% behind the wetting front. The water pressure just behind the wetting front for the water wettable sand was −0.10 m as shown in Figs. 7 and 8. For the water-repellent sand the water pressure just behind the wetting front was simulated to be about 0.071 m as shown in Figs. 7 and 9. This positive pressure behind the wetting front for the water-repellent sand is expected since for the extremely water repellent case the water entry pressure is about 0.045 m.

The comparison between the experimental and the numerical simulation results are quite good. Additional parameter characterization would be helpful to improve the degree of agreement between the simulated and experimental results. The main parameter

that needs to be quantified independently is the water saturation—unsaturated hydraulic conductivity relationship. In the present study we assumed that the unsaturated hydraulic conductivity function could be predicted by the Van Genuchten (1980) equations along with the measured saturated hydraulic conductivity.

Although the drainage flux at the bottom of the flow domain was not reported by Bauters et al. (1998), it is worthwhile to examine this flux as the timing and the magnitude of this flux affect the potential transport of constituents through the porous medium. Drainage flux at the bottom of the flow domain occurs after the wetting front reaches the bottom boundary and the pressure at the exit point reaches zero. The drainage fluxes for the two cases considered here are illustrated in Fig. 10. As expected the initiation of drainage flux occurs much sooner for the unstable case in comparison to the stable flow case. The initiation for the unstable flow case occurs about 3400 s ahead of the initiation of drainage flux for the stable flow case.

The maximum drainage flux is momentarily much higher for the unstable flow case. The sharp peak in drainage flux for the unstable flow case occurs due to the storage of water behind the fingertip. This storage occurs because of the water repellency at the fingertip, and once the fingertip breaks through the bottom boundary, the stored water is released rapidly. Following the sharp peak in drainage flux, the flux decreases exponentially to the steady rate determined by the applied flux.

The influence of preferential flow through fingers on solute transport is similar to preferential flow in macropores (Nieber and Misra, 1995). The character of the impact depends on whether the chemical is dissolved in the applied water or initially incorporated in the porous medium. The faster breakthrough of water at the bottom boundary for the unstable flow case is indicative of conditions that will favor more rapid transport of chemicals initially dissolved in the applied water. For situations where a chemical is initially incorporated in the porous medium the chemical will also break through more rapidly for the unstable case. However, the amount leached for the unstable flow case is potentially less than that leached for the stable flow case since for the stable flow case the flow sweeps the entire porous domain. We say is it potentially less because the stable flow case requires a much longer time to produce leachate, thereby providing more opportunity for reactive chemicals to be consumed.

Overall, we can conclude that water repellency has a significant influence on the spatial pattern of flow and the timing of flow. The results presented here illustrate the potential detrimental impact of unstable flow on moisture and chemical distributions in soils. The unstable flow process has the potential to increase the rate of leaching of chemicals to ground water, but simultaneously it will decrease the availability of water and nutrients to plants.

In the present study we only examined the case of extreme water repellency. In addition to the results examined here, the laboratory data of Bauters et al. (1998) include results for both slightly and severely water repellent sands. Additional simulation work remains to be done to test the effect of the degree of water repellency on the characteristics of unstable flows.

6. Summary and conclusions

A finite element numerical solution of the Richards equation was applied to the simulation of water flow in a two-dimensional region of sand for two conditions. For one condition the sand was completely water wettable, while in the other case the sand was extremely water repellent. Experimental measurements in a laboratory chamber for the two conditions yielded stable flow for the water wettable condition and unstable flow for the water-repellent condition. Water saturation—capillary pressure relations for the two sand conditions were measured experimentally for both the main wetting curve and the main drainage curve. These relations, along with the measured saturated hydraulic conductivity of the sand were used in the numerical solutions.

Characteristics compared between the numerical simulation and the experimental measurements included the temporal pressure distribution at a selected point in the domain, wetting front travel times, and the general description of the saturation distribution within the domain at selected times. The numerical solution predicted a stable-wetting front for the water wettable sand, and this was in agreement

with the experimental result. The temporal change in pressure at a selected point was very similar for the numerical simulation and the experimental measurement. The velocity of the simulated wetting front was similar to that measured in the laboratory experiment.

The numerical simulation correctly predicted an unstable flow condition for the extremely water repellent sand. The width of the finger formed and its average velocity of propagation were both similar to those measured in the laboratory experiment. The temporal distribution of the pressure at a selected point within the finger was very similar to that measured in the laboratory experiment.

Overall, the characteristics of the simulated unstable flow were true to the conditions that have been derived from experimental measurements. As a result we can conclude that the numerical simulation model appears to be a valid tool to study gravity-driven unstable flows in water repellent porous media. However, additional simulations remain to be completed to more fully test the effect of degree of water repellency on the characteristics of unstable flows.

Acknowledgements

Published as Paper No. 991120036 of the scientific journal series of the Minnesota Agricultural Experiment Station on research conducted under Minnesota Agricultural Experiment Station Project No. 12-047. This work was also supported by the Army High Performance Computing Research Center under the auspices of the Department of the Army, Army Research Laboratory cooperative agreement number DAAH04-95-2-0003/contract number DAAH04-95-C-0008, the content of which does not necessarily reflect the position or the policy of the government, and no official endorsement should be inferred.

References

Bauters, T.W.J., DiCarlo, D.A., Steenhuis, T.S., Parlange, J.-Y., 1998. Preferential flow in water-repellent sands. Soil Sci. Soc. Am. J. 62, 1185–1190.

Bauters, T.W.J., Steenhuis, T.S., DiCarlo, D.A., Nieber, J.L., Dekker, L.W., Ritsema, C.J. Parlange, J.-Y., 2000. Physics of water repellent soils, J. Hydrol. 231–232, 233–243.

Beven, K., Germann, P., 1982. Macropores and water flow in soils. Water Resour. Res. 18, 1311–1325.

Birkholzer, J., Tsang, C.-F., 1997. Solute channeling in unsaturated heterogeneous porous media. Water Resour. Res. 33, 2221–2238.

Dekker, L.W., Ritsema, C.J., 1996. Preferential flow paths in a water repellent clay soil with grass cover. Water Resour. Res. 32, 1239–1249.

De Rooij, G.H., 1995. A three-region analytical model of solute leaching in a soil with a water-repellent top layer. Water Resour. Res. 31, 2701–2707.

De Rooij, G.H., De Vries, P., 1996. Solute leaching in a sandy soil with a water-repellent surface layer: a simulation. Geoderma 70, 253–263.

Glass, R.J., Parlange, J.-Y., Steenhuis, T.S., 1989a. Wetting front instability, 2. Experimental determination of relationships between system parameters and two-dimensional unstable flow field behavior in initially dry porous media. Water Resour. Res. 25, 1195–1207.

Glass, R.J., Steenhuis, T.S., Parlange, J.-Y., 1989b. Mechanism for finger persistence in homogeneous, unsaturated, porous media: Theory and verification. Soil Sci. 148, 60–70.

Hendrickx, J.M.H., Dekker, L.W., Boersma, O.H., 1993. Unstable wetting fronts in water-repellent field soils. J. Environ. Qual. 22, 109–118.

Jamison, V.C., 1945. The penetration of irrigation and rain water into sandy soil of Central Florida. Soil Sci. Soc. Am. Proc. 10, 25–29.

Kung, K.-J. S., 1990. Preferential flow in a sandy vadose zone soil, 2. Mechanism and implications. Geoderma 46, 59–71.

Liu, Y., Steenhuis, T.S., Parlange, J.-Y., 1994. Formation and persistence of fingered flow in coarse grained soils under different moisture contents. J. Hydrol. 159, 187–195.

Mualem, Y., 1974. A conceptual model of hysteresis. Water Resour. Res. 10, 514–520.

Nguyen, H.V., Nieber, J.L., Ritsema, C.J., Dekker, L.W., Steenhuis, T.S, 1999. Modeling gravity-driven unstable flow in a water repellent soil. J. Hydrol. 215, 202–214.

Nieber, J.L., 1996. Modeling finger development and persistence in initially dry porous media. Geoderma 70, 209–229.

Nieber, J.L., Misra, D., 1995. Modeling flow and transport in heterogeneous, dual-porosity drained soils. Irrig. Drain. Syst. 9, 217–237.

Parker, J.C., 1989. Multiphase flow and transport in porous media. Rev. Geophys. 27, 312–328.

Raats, P.A.C., 1973. Unstable wetting fronts in uniform and non-uniform soils. Soil Sci. Soc. Am. Proc. 37, 681–685.

Ritsema, C.J., Dekker, L.W., 1994. How water moves in a water repellent sandy soil, 2. Dynamics of fingered flow. Water Resour. Res. 30, 2519–2531.

Ritsema, C.J., Dekker, L.W., Hendrickx, J.M.H., Hamminga, W., 1993. Preferential flow mechanism in a water-repellent sandy soil. Water Resour. Res. 29, 2183–2193.

Ritsema, C.J., Dekker, L.W., Nieber, J.L., Steenhuis, T.S., 1998. Modeling and field evidence of finger formation and finger

recurrence in a water repellent sandy soil. Water Resour. Res. 34, 555–567.

Roth, K., 1995. Steady state flow in an unsaturated, two-dimensional macroscopically homogeneous, Miller-similar medium. Water Resour. Res. 31, 2127–2140.

Selker, J.S., Steenhuis, T.S., Parlange, J.-Y., 1992. Fingered flow in two dimensions. 1. Measurement of matric potential. Water Resour. Res. 28, 2513–2521.

Van Dam, J.C., Hendrickx, J.M.H., Van Ommen, H.C., Bannink, M.H., Van Genuchten, M.Th., Dekker, L.W., 1990. Water and solute movement in a coarse-textured water-repellent field soil. J. Hydrol. 120, 359–379.

Van Genuchten, M.Th., 1980. A closed-form equation for predicting the hydraulic conductivity of unsaturated soils. Soil Sci. Soc. Am. J. 44, 892–898.

Van Genuchten, M.Th., Leij, F.J., Yates, S.R., 1991. The RETC code for quantifying the hydraulic functions of unsaturated soils, EPA/600/2-91/065. 93pp. R.S. Kerr Environ. Res. Lab., US Environmental Protection Agency, Ada, OK.